LANGMUIR

pubs.acs.org/Langmuir Article

Missing Piece in Colloidal Stability—Morphological Factor of Hydrophobic Nanoparticles

Chin-Yi Chen, Meng-Ju Hsieh, Ankit Raj, Wei-Cheng Peng, Hiro-o Hamaguchi, Wei-Tsung Chuang, Xiaosong Wang,* and Chien-Lung Wang*

Cite This: *Langmuir* 2023, 39, 2922–2931 Read Online

ACCESS | Metrics & More | Article Recommendations | Supporting Information

ABSTRACT: Hydrophobic nanoparticles (NPs) in water were considered unstable because they lack the repulsive electrostatic interaction and steric effect to prevent aggregation. In this study, porous hydrophobic NPs of two star-shaped giant molecules, **POSS-(R)$_8$**, were found to be stable in water and able to retain their kinetic stability in a wide range of temperatures, pH values, and ionic strengths. Unlike the solid hydrophobic NPs that aggregate even with the negative zeta potential (ζ) induced by surface-structured hydrogen-bonded (SHB) water, the porous morphology of **POSS-(R)$_8$** NPs reduces the entropically driven hydrophobic effect to prevent aggregation. With the porous morphology, the hydrophobic NPs are stable without the hydrophilic or charged surface functional groups and demonstrate good encapsulation capability. The morphological factor of colloids is thus one of the missing pieces in the theory of colloidal stability that extends our understanding of colloidal science.

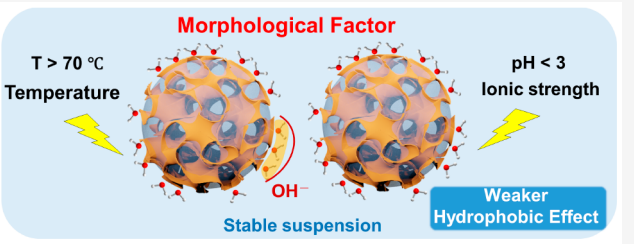

INTRODUCTION

Colloidal stability in water is an essential factor in nanoscience and nanotechnology. To deliver proper functions, synthetic nanoparticles (NPs) should maintain particle structures and defer aggregation before they reach the targeted areas.[1−7] The earliest mechanism of colloidal stability in the dispersing medium was proposed in 1941 and now is well-known as the Deryaguin−Landau−Verwey−Overbeek (DLVO) theory.[8,9] The theory explains that NPs with surface charges arose from ionic groups of surfactants or surface modification can be stably dispersed in water because the potential energy that originated from the repulsive electrostatic interaction (V_{elec}) overwhelms the attractive van der Waals interaction (V_{vdW}). As a result, $V_{DLVO} = V_{elec} + V_{vdW} > 0$ indicates an overall repulsive interaction that prevents particle aggregation and enables colloidal stability. Neutral NPs, which lack repulsive interaction V_{elec}, can be stabilized by steric interaction (V_{st}). Examples include NPs of block and graft copolymers, which are stable in water because the hydrophobic segments assemble to form an inner hydrophobic core that is surrounded by the strongly hydrated hydrophilic segments and extend into the aqueous phase to form the steric shell necessary for stabilization.[10] To also include the steric contribution V_{st}, the DLVO theory was suitably augmented with a steric term: $V_{DLVO} = V_{elec} + V_{st} + V_{vdW}$.[11−13] Therefore, repulsive V_{elec} and V_{st} are commonly recognized as the source for the colloidal stability in water, which inspired scientists to promote repulsive interactions via surface chemistry to create a stable monodisperse system.[14,15]

Zeta potential (ζ) is a commonly used quantity for the degree of electrostatic repulsion among NPs. NPs with $\zeta > |\pm 40|$ mV are normally considered as stable colloids in water.[16] It is well-known that ζ of the surfactant colloids is contributed from the ionic groups of the surfactant molecules, but it is less known that NPs of hydrophobic molecules also possess negative ζ in water. Although the electronic and molecular origins of negative ζ at the oil/water interface have not been fully understood,[17−19] it is generally accepted that the surface of hydrophobic NPs can possess a negative ζ in water, because the hydrophobic surface of the NPs either induces structured hydrogen-bonded (SHB) water to attract OH^- ions or allows the charge transfer to occur, thereby generating negative ζ of hydrophobic NPs.[20−22] It is quite amazing that researchers have found that the oil droplets of xylene, dodecane, hexadecane, and perfluoromethyldecalin actually have ζ as negative as −50 to −60 mV when their particle diameters are around 100−200 nm.[17] Simply considering V_{DLVO}, with such negative ζ, the electrostatic repulsion of these NPs is supposed to maintain the stability of the hydrophobic NPs. Nevertheless, in reality, even with such negative ζ, the NPs of hydrophobic molecules are not stable in water and still aggregate until the

Received: September 20, 2022
Revised: January 30, 2023
Published: February 14, 2023

https://doi.org/10.1021/acs.langmuir.2c02582
Langmuir 2023, 39, 2922−2931

Scheme 1. (a) Schematic Illustration for the Proposed Morphological Engineering That Reduces the Hydrophobic Effect of Hydrophobic NPs and (b) Chemical Structures of the Star-Shaped Molecules, POSS-Hept and POSS-Ad, and Their Building Blocks, Octakis(dimethylsilyloxy)-Substituted Polyhedral Oligomeric Silsesquioxane, Octane, and Adamantane

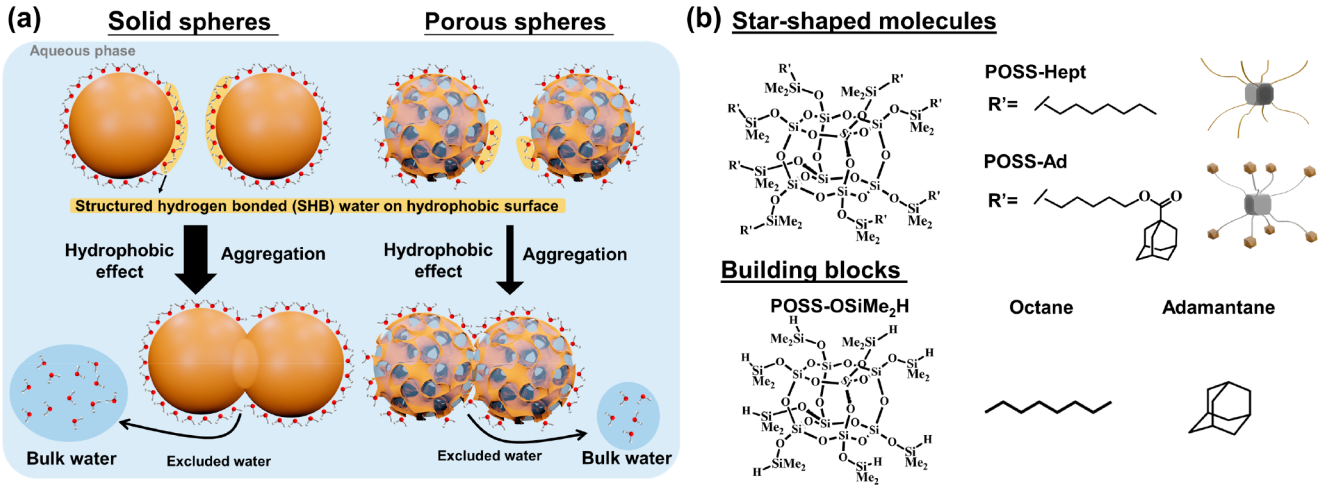

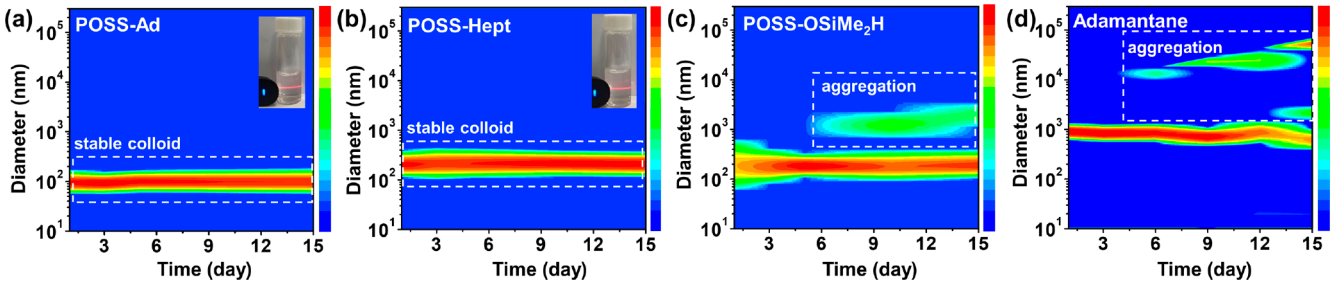

Figure 1. Time-dependent DLS analysis of (a) **POSS-Ad**, (b) **POSS-Hept**, (c) **POSS-OSiMe$_2$H**, and (d) adamantane.

hydrophobic molecules are phase-separated or precipitate from water.

One driving force that causes hydrophobic molecules to aggregate and phase separate from water is known as the "hydrophobic effect".[23−25] This entropically driven process causes the aggregation of hydrophobic segments in water by freeing the SHB water on the hydrophobic segments into bulk water. Because most hydrophobic molecules eventually aggregate into large particles or sediments in water, it is reasonable to believe that the hydrophobic effect can overwhelm the negative ζ of the hydrophobic NPs induced by the surface-structured water to facilitate aggregation. However, in this case, it is difficult to apply the DLVO theory to understand why ζ of the ionic NPs can counter the attractive V_{vdW} and maintain the colloidal stability but ζ of the NPs of the hydrophobic molecules cannot. Thus, the fact that the repulsive electrostatic interaction of hydrophobic NPs fails to maintain the colloidal stability indicates that, in addition to the energy aspects from the attractive and repulsive interactions in the DLVO theory, there could be more unknown factors in the mechanism of colloidal stability.

Although phase separation or precipitation of hydrophobic materials in water is commonly expected, unexpected colloidal stability of hydrophobic materials does exist. Without surface modification, Yang et al. reported a novel type of highly monodispersed stable raspberry-like colloids;[26] Pashley found that the removal of dissolved gas increases the stability of colloids;[27] and Rossitza et al. found high stability of fullerene colloids in polar organic solvents with negative surface potential, although the origins were not explained.[28] These cases inspired us to explore suitable molecular designs that lead to a stabilization mechanism supplemental to the DLVO theory. Because aggregation caused by the hydrophobic effect is an entropically driven process and cannot be stopped by the electrostatic repulsion, hydrophobic NPs need additional features to diminish the hydrophobic effect. To achieve that, instead of enhancing the repulsive interaction, we looked for the morphological factors that can minimize the loss of the structured water molecules when NPs collapse with each other. Because the hydrophobic effect is driven by the entropy increase caused by freeing the structured water molecules, as illustrated in Scheme 1a, the amount of surface-structured water molecules can be decreased if hydrophobic NPs are morphologically engineered into porous NPs. The porous morphology may reduce the amount of structured water molecules freed from the collision of porous NPs, so that the entropically driven hydrophobic effect can be weakened and the concept of morphological stability of hydrophobic NPs may be established. The porous hydrophobic NPs in this study are made by the aggregation of the neutral and water-insoluble star-shaped giant molecules [**POSS-(R)$_8$** in Scheme 1b]. The two star-shaped molecules, **POSS-Hept** and **POSS-Ad**, are difficult to be closely packed and have different peripheral groups, flexible heptyl chains (-Hept) versus rigid adamantyl end units (-Ad). In this case, the aggregation of the **POSS-(R)$_8$** molecules in water may result in different types of hydrophobic pockets and enable different degrees of morphological engineering to the resulting porous hydrophobic NPs. By

https://doi.org/10.1021/acs.langmuir.2c02582
Langmuir 2023, 39, 2922−2931

characterization of the structures and examination of the stability of the hydrophobic NPs, the correlation between the morphology and stability of the NPs was built to reveal the essential factor in the morphological stability of hydrophobic NPs. It was found that energy aspects in the classical DLVO theory cannot be applied to explain the colloidal stability of the porous hydrophobic NPs. Instead, the limited hydrophobic surface area on the porous NPs weakens the hydrophobic effect and stabilizes the hydrophobic NPs. The finding provides a new aspect in preparing stable hydrophobic NPs in water and reveals a morphological factor as one of the missing pieces in the mechanism of colloidal stability.

RESULTS AND DISCUSSION

The synthetic routes and characterization data of **POSS-Hept** and **POSS-Ad** are shown in Scheme S1 and Figures S6–S11 and described in the Supporting Information. The **POSS-(R)$_8$** NPs in water were prepared by adding 10 mL of water quickly into 1 mL of the tetrahydrofuran (THF) solutions (1 mg/mL) of **POSS-(R)$_8$**, followed by dialysis of the solutions against water (0.5 L, 3 times) to remove THF. The time-dependent dynamic light scattering (DLS) analysis of the colloids is shown in Figure 1, and the characteristics of the colloids are summarized in Table 1. As shown in panels a and b of Figure 1, the **POSS-(R)$_8$** colloids were fairly stable because their hydrodynamic diameter (D_h) and polydispersity (PDI) as characterized by DLS remaining unchanged over 15 days. In contrast, without the peripheral groups, the core unit [octakis(dimethylsilyloxy)-substituted polyhedral oligomeric silsesquioxanes, **POSS-OSiMe$_2$H**] formed a less stable colloidal solution that started to aggregate and form larger particles with $D_h \sim 1400$ nm on the sixth day (see Figure 1c). The peripheral adamantane unit alone is also unstable, because the as-prepared colloidal solution of adamantane already gave a large particle size ($D_h \sim 980$ nm) and formed aggregates on the fourth day, as shown in Figure 1d. The results demonstrate that the hydrophobic NPs require the star-like geometry of **POSS-(R)$_8$** that contains both the POSS core and the eight peripheral groups to form the kinetically stable colloids.

Table 1. Characteristics of the POSS-(R)$_8$ Colloids in Water[a]

	D_h (nm)	PDI	ζ (mV)
POSS-Hept	201 ± 20.1	0.22 ± 0.01	−56.9 ± 1.4
POSS-Ad	103 ± 15.8	0.07 ± 0.03	−20.1 ± 2.3

[a]The colloids have undergone dialysis against water for 24 h, with water replaced 3 times.

Table 1 summarized D_h, PDI, and ζ of the two **POSS-(R)$_8$** colloids. Although these two star-like molecules are neutral in charge, negative ζ of −56.9 and −20.1 mV were measured from the colloidal solutions of **POSS-Hept** and **POSS-Ad**. Previous studies show that the surface density of SHB water decreases and ζ becomes less negative with increasing radius (or equivalently with decreasing curvature)[29] of non-porous hydrophobic NPs.[30] In Figure S12 of the Supporting Information, time-dependent ζ of the sonicated *o*-xylene$_{(l)}$ in water also shows that ζ of the *o*-xylene droplets decreases with the increasing size of droplets. Although it was not surprising to observe that both **POSS-(R)$_8$** NPs possess negative ζ, it is quite strange to see that the **POSS-Ad** NPs possess a less negative ζ with the smaller D_h. Because the colloidal solutions of **POSS-Hept** and **POSS-Ad** were prepared at the same concentration (0.1 mg/mL), the smaller D_h of **POSS-Ad** was expected to result in a higher ζ than **POSS-Hept** in water. Moreover, the fact that **POSS-Ad** maintains a smaller D_h and PDI with a less negative ζ (−20.1 mV) was also counter-intuitive, because in the DLVO theory,[8,9] the better kinetic stability should be achieved by the higher ζ of the colloids. Therefore, the colloidal characteristics shown in Table 1 seem to suggest that the **POSS-(R)$_8$** NPs are morphologically different from the solid spherical NPs and the mechanism behind their colloidal stability cannot be simply explained by the classical DLVO theory.

To reveal the possible mechanism of the unexpected colloidal stability, Raman spectroscopy with the data analyzed by the hypothetical addition multivariate analysis with numerical differentiation (HAMAND)[31,32] was used to produce the solute-correlated (SC) spectra that reveal the structural features of water molecules that are perturbated by

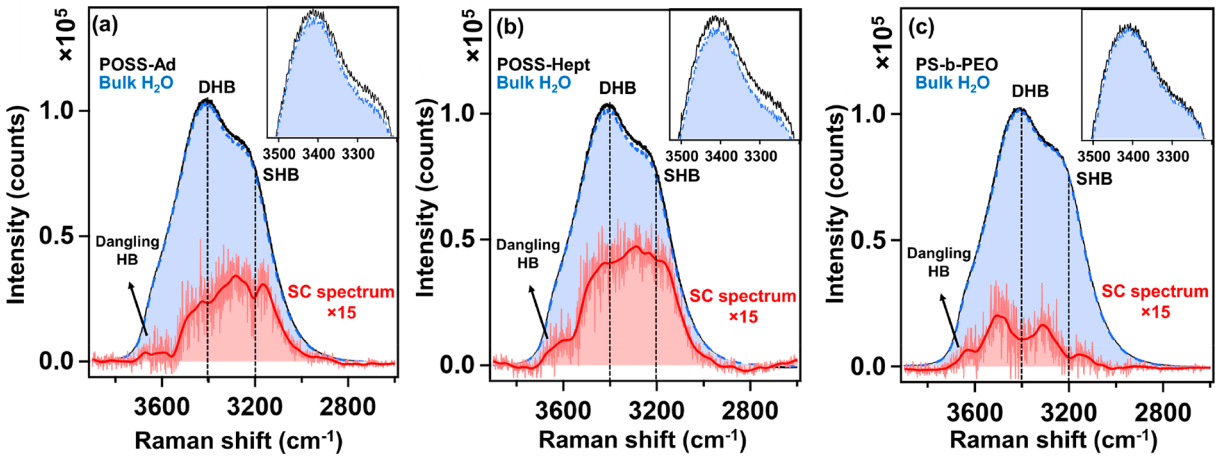

Figure 2. Raman scattering and SC spectra for the colloidal solution of (a) **POSS-Ad**, (b) **POSS-Hept**, and (c) **PS-*b*-PEO**. The SC spectra are enlarged by 15 times. The expanded view of the Raman spectra for bulk water and the colloidal solutions were also included in the inset. The wavenumber around 3630, 3400, and 3200 cm^{-1} shows the vibration of dangling (non-hydrogen bonded) −OH, DHB water, and SHB water, respectively. The smoothed spectra were obtained using the Savitzky–Golay filter and shown as the red lines in the panels.

https://doi.org/10.1021/acs.langmuir.2c02582
Langmuir 2023, 39, 2922–2931

the hydrophobic NPs. Along with the Raman spectra of bulk water, the spectra of the two **POSS-(R)$_8$** colloidal solutions are shown in panels a and b of Figure 2. According to the literature,[33,34] dangling (non-hydrogen bonded) −OH, destructured hydrogen-bonded (DHB) water, and SHB water give Raman scattering at 3630, 3400, and 3200 cm^{-1}, respectively. The ratio of SHB water to DHB water should be a measure of the "structurality" of water under ambient conditions.[35] In bulk water, each water molecule owns 3.6 hydrogen bonds on average;[24] therefore, the typical Raman spectrum of bulk water shows higher Raman scattering intensity at 3400 cm^{-1} (from the DHB water) than at 3200 cm^{-1} (from the SHB water). In contrast, in the SC spectra of **POSS-Ad** and **POSS-Hept**, the relative Raman intensity of the DHB water was significantly diminished, whereas that of the SHB water was enhanced. It has been known that water molecules on the hydrophobic surface form the hydrogen-bond network and are tetrahedrally coordinated.[24,25,34,36−38] The higher Raman intensity of the SHB water thus indicates that the two **POSS-(R)$_8$** hydrophobic NPs provide the more hydrophobic interface with water to induce the formation of the SHB water. Because it is known that surface charges can be induced from the SHB water on the surface area of hydrophobic NPs,[17−19] the observation of the SHB water in the SC spectra of the two **POSS-(R)$_8$** hydrophobic NPs explains why both **POSS-Hept** and **POSS-Ad** NPs have negative ζ. In Figure 2c, the Raman spectrum of a polystyrene-*block*-polyethylene oxide (**PS-*b*-PEO**) colloidal solution (D_h = 102.6 nm and PDI = 0.177) was also measured and used as the reference that represents classic amphiphilic NPs for comparison. In comparison to the colloidal solutions of POSS-(R)$_8$, the Raman spectra of **PS-*b*-PEO** overlaps better with that of the bulk water, leading to the weaker SC spectrum, which contains more DHB water than the SHB water. In Figure S13 of the Supporting Information, the SC spectrum of the tetraethylene glycol (TEG) aqueous solution also shows a similar feature. These results show that classic NPs, like the **PS-*b*-PEO** NPs, may use mainly the hydrophilic PEO shell instead of the hydrophobic PS core to interact with water.

Although the observation of the SHB water clarifies the source of negative ζ of the **POSS-(R)$_8$** NPs, the results did not explain why the **POSS-Hept** NPs have a more negative ζ than the **POSS-Ad** NPs (−56.9 mV versus −20.1 mV). As seen in Figure S12 of the Supporting Information, for solid spherical NPs, such as the hydrophobic *o*-xylene droplets, their ζ becomes less negative with the increasing size of droplets. The situation in the **POSS-(R)$_8$** NPs is completely opposite because the **POSS-Ad** NPs, which have a smaller D_h, possess a less negative ζ compared to the larger **POSS-Hept** NPs. One of the possibilities to cause such contradiction may come from the morphological factor of the **POSS-(R)$_8$** NPs.

In fact, the Raman scattering of the perturbed water molecules in the SC spectra can originate from both the surface and interstitial water, meaning that the SHB water could locate on the surface or in the internal hydrophobic pockets of the hydrophobic NPs. With the knowledge that the intensity of a Raman band depends linearly upon the concentration of the related functional group, the integral areas in the SC spectra of the two **POSS-(R)$_8$** NPs (see the red areas in panels a and b of Figure 2) were used to estimate the number of water molecules that are perturbated by the hydrophobic NPs. The relative area in the SC spectra of **POSS-Hept** and **POSS-Ad** was found to be 1.52:1, indicating that the **POSS-Hept** NPs perturbate more water molecules than the **POSS-Ad** NPs. If a morphological model of a solid sphere is applied, NPs with a larger D_h should perturb both fewer water molecules per unit area, which should lead to a less negative ζ and fewer water molecules per volume of solution because of their lower area/volume ratio and lower number of particles per volume of solution. Perturbing fewer water molecules per volume of solution would lead to a lower area below the SC spectra. The fact that the **POSS-Hept** NPs perturb more water molecules with a larger D_h thus disproves the solid sphere model and suggests that the **POSS-(R)$_8$** NPs could be porous NPs that contain internal hydrophobic pockets to host interstitial water.

To produce more perturbated water molecules at a larger D_h, a porous NP has to utilize smaller pores to compensate for its deficient surface/volume ratio. In combination of the characterization results from the DLS, ζ, and Raman spectra, the porous NP models of **POSS-Hept** and **POSS-Ad** were proposed in Figure 3. The model shows that, in comparison to

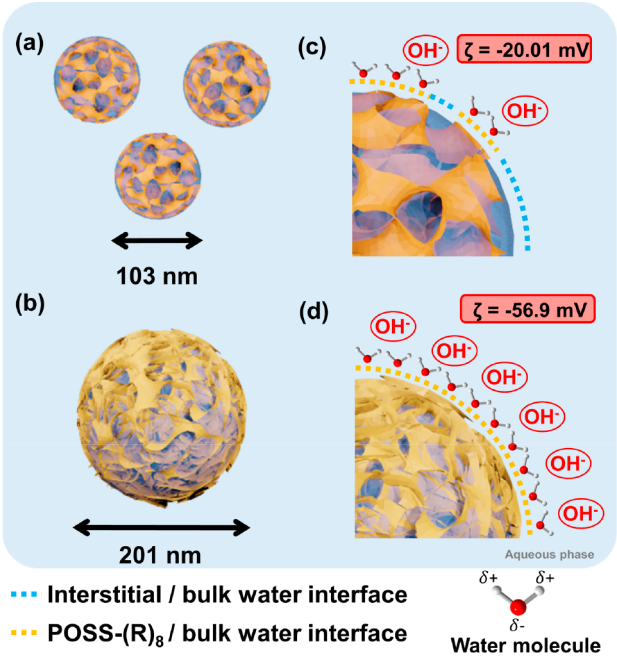

Figure 3. Porous NP models representing the size of (a) **POSS-Ad** and (b) **POSS-Hept** NPs. The surface charges that can be induced on the (c) **POSS-Ad** and (d) **POSS-Hept** NPs.

POSS-Ad, although the **POSS-Hept** NP has a larger D_h (panels a and b of Figure 3), its smaller hydrophobic pores could result in a larger internal hydrophobic area to induce more SC water molecules (see panels c and d of Figure 3). In contrast, although the **POSS-Ad** NP has a smaller D_h, its larger pore size may reduce the surface area of the hydrophobic NP and lead to a less negative ζ.

To result in different pore sizes, **POSS-Hept** and **POSS-Ad** should form different aggregated morphology. **POSS-Hept** and **POSS-Ad** are both viscous liquids. The weaker scattering halos of pure **POSS-Hept$_{(l)}$** in Figure 4a indicate that **POSS-Hept** forms more disorder and weaker aggregates than **POSS-Ad** in the liquid state. In the aqueous colloidal solution, the scattering halos of **POSS-Hept** observed in the condensed phase are gone, as shown in Figure 4b. Only a weak scattering halo at q = 1.4−2.2 Å^{-1} (d spacing = 4.5−2.9 Å) originating from the

https://doi.org/10.1021/acs.langmuir.2c02582
Langmuir 2023, 39, 2922−2931

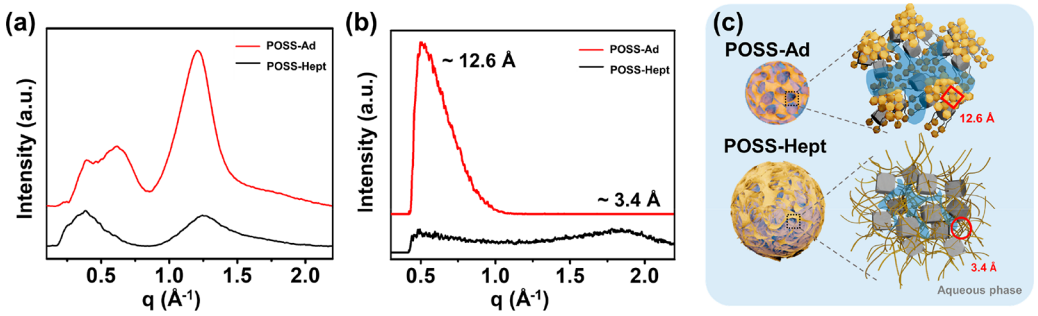

Figure 4. Wide-angle X-ray scattering (WAXS) profiles of the (a) pure liquids and (b) aqueous colloidal solutions of **POSS-Ad** and **POSS-Hept**. (c) Illustration of the proposed aggregated structures of **POSS-Ad** and **POSS-Hept** in the colloidal solutions. The concentration of **POSS-(R)$_8$** in the colloidal solution is 0.1 mg/mL.

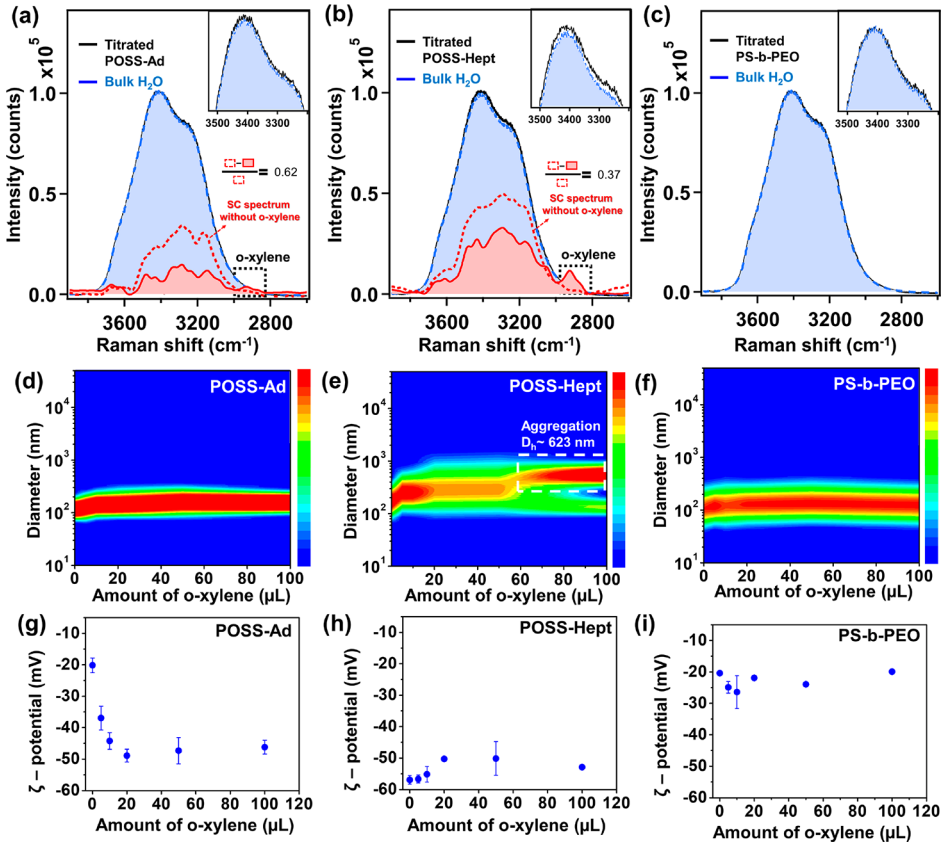

Figure 5. (a–c) Raman scattering and SC spectra of the **POSS-Ad**, **POSS-Hept**, and **PS-*b*-PEO** colloidal solutions after 100 μL of *o*-xylene$_{(l)}$ was added to the 1 mL colloidal solutions. (d–f) Size distribution and (g–i) ζ of the *o*-xylene$_{(l)}$-titrated **POSS-Ad**, **POSS-Hept**, and **PS-*b*-PEO** colloidal solutions in the dynamic swelling experiment. In the experiment, *o*-xylene$_{(l)}$ was added to the 1 mL colloidal solution (0.1 mg/mL). The SC spectra are enlarged by 15 times. The expanded views of Raman spectra for bulk water and the colloidal solution are shown in the top right inset. The dashed box from 2800 to 3100 cm^{-1} shows the C–H stretching vibration of *o*-xylene$_{(l)}$. The ratio of the expelled SC water was calculated on the basis of the integral area of the SC spectra before and after the *o*-xylene$_{(l)}$ titration. The results show that 62% of SC water was expelled from the **POSS-Ad** NPs and 37% of SC water was expelled from the **POSS-Hept** NPs.

short-ranged ordered aggregates of the peripheral alkyl groups was observed.[39] In contrast, the colloidal solution of **POSS-Ad** shows a strong scattering band at q = 0.6 Å^{-1} (d spacing = 12.6 Å), suggesting that the POSS core and the peripheral Ad units of POSS-Ad remain strongly aggregated in the colloidal solution to give the quasi-long-ranged order packing with a d spacing = 12.6 Å. The strongly aggregated core and peripheral units in the hydrophobic NPs could lead to the stronger microphase separation with water in the **POSS-Ad** NPs and result in the larger pore size, as illustrated in Figures 3c and 4c. In contrast, in the POSS-Hept NPs, the core units are randomly separated by the peripheral heptyl chains, so that the scattering halo at the lower angle was not found. The only weak scattering halo at q = 1.4–2.2 Å^{-1} suggests that the peripheral heptyl chains loosely aggregate to hold the hydrophobic NPs. In this case, as a result of the randomly distributed core units and the loosely aggregated peripheral groups, the **POSS-Hept** NPs, which have a larger D_h, possess smaller hydrophobic pores to provide a more internal hydrophobic area that perturbs more water molecules to give a stronger SC Raman spectrum in Figure 2b. The porous model of the **POSS-Ad** NPs can also be used to rationale its

https://doi.org/10.1021/acs.langmuir.2c02582
Langmuir 2023, 39, 2922–2931

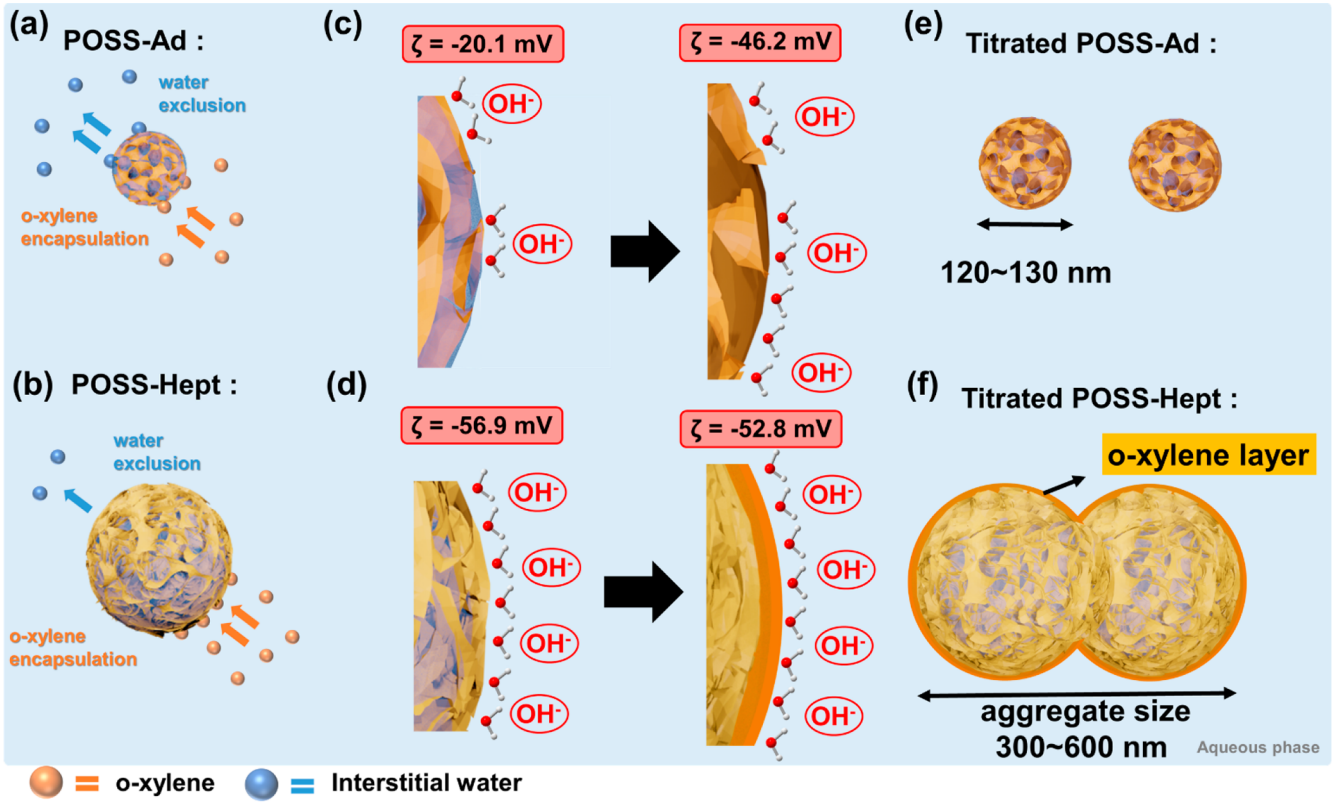

Figure 6. Schematic illustrations of (a and b) responses to the *o*-xylene titration process, (c and d) ζ and morphological changes caused by the *o*-xylene titration, and (e and f) final particle sizes of the **POSS-Ad** and **POSS-Hept** NPs.

less negative ζ, because the tightly aggregated units decrease the hydrophobic surface area and reduce the SHB water molecules and surface charges that can be induced on the **POSS-Ad** NPs, as also illustrated in Figure 3c. As for the colloidal stability, it is worth noting that parts of the interparticle collisions of porous NPs involve simply the contact of the hydrophobic pockets of NPs. This type of contact does not result in the release of SHB water molecules. Thus, the entropy-driven hydrophobic effect is less effective in causing aggregation as a result of the morphological feature of porous NPs. In combination of all of the structural analysis, it is believed that the unique colloidal characteristics and stability of two porous hydrophobic **POSS-(R)$_8$** NPs originated from the morphological factor, which could be a missing piece supplemental to the classical mechanism of colloidal stability.

The morphological differences in the **POSS-Ad**, **POSS-Hept**, and classical **PS-*b*-PEO** NPs can be further reflected by the different encapsulation behaviors of the NPs tested in the dynamic swelling experiment,[40] where the NPs were treated as the seed particles and their Raman spectra, size distribution, and ζ were examined when various amounts of *o*-xylene$_{(l)}$ were added to 1 mL of the colloidal solutions (0.1 mg/mL). In the experiment, hydrophobic *o*-xylene$_{(l)}$ acts as the morphological modifier that fills the hydrophobic pockets or covers the hydrophobic surface of the NPs. The subsequent changes in the Raman spectra, size distribution, and ζ of the *o*-xylene$_{(l)}$-titrated colloidal solutions can then be analyzed to reveal the morphological changes. The SC Raman spectra of the *o*-xylene$_{(l)}$-titrated colloidal solutions were analyzed and shown in panels a–c of Figure 5. In comparison of the SC spectra before and after the *o*-xylene$_{(l)}$ titration, it can be found that **POSS-Ad** NPs lost a higher ratio of the SC water (62%) than the **POSS-Hept** NPs (37%). To expel more SC water from the **POSS-(R)$_8$** NPs, the *o*-xylene$_{(l)}$ molecules have to diffuse into the internal hydrophobic pockets of the **POSS-(R)$_8$** NPs and free the interstitial water molecules. The higher decrease in the SC water of the **POSS-Ad** solution thus suggests that the interstitial water located in the hydrophobic pockets of the **POSS-Ad** NPs can be more easily replaced by the hydrophobic *o*-xylene$_{(l)}$ molecules. This finding goes along with the models in Figure 3, where the larger pore size of the **POSS-Ad** NPs facilitates the encapsulation of the hydrophobic *o*-xylene$_{(l)}$ molecules. As for the **PS-*b*-PEO** NPs, the addition of *o*-xylene$_{(l)}$ did not change the Raman spectra, indicating that, as a result of the lack of a porous core and the steric effect of the hydrophilic PEO shell, this classical amphiphilic NP is more difficult to encapsulate added *o*-xylene$_{(l)}$.

The encapsulation of the *o*-xylene$_{(l)}$ molecules could alter the morphological features of the NPs and, consequently, affect the colloidal stability. In panels d–f of Figure 5, the two-dimensional (2D) size distribution diagrams show that the **POSS-(R)$_8$** NPs and the **PS-*b*-PEO** NPs responded differently to added *o*-xylene$_{(l)}$. Added *o*-xylene$_{(l)}$ did not affect the colloidal stability of **PS-*b*-PEO** NPs because they are stabilized mainly by the steric effect provided by the PEO segments. However, as seen in panels d and e of Figure 5, for the hydrophobic **POSS-(R)$_8$** NPs that are mainly stabilized by their morphological features, added *o*-xylene$_{(l)}$ can cause very different responses. Below the adding amount of 50 μL, added *o*-xylene$_{(l)}$, although swelling the **POSS-Ad** and **POSS-Hept** NPs, did not cause aggregation. Nevertheless, when the adding amount of *o*-xylene$_{(l)}$ is higher than 50 μL, while the **POSS-Ad** NPs still hold the size distribution, the **POSS-Hept** NPs lose their colloidal stability and start to aggregate. Panels g–i of

https://doi.org/10.1021/acs.langmuir.2c02582
Langmuir 2023, 39, 2922–2931

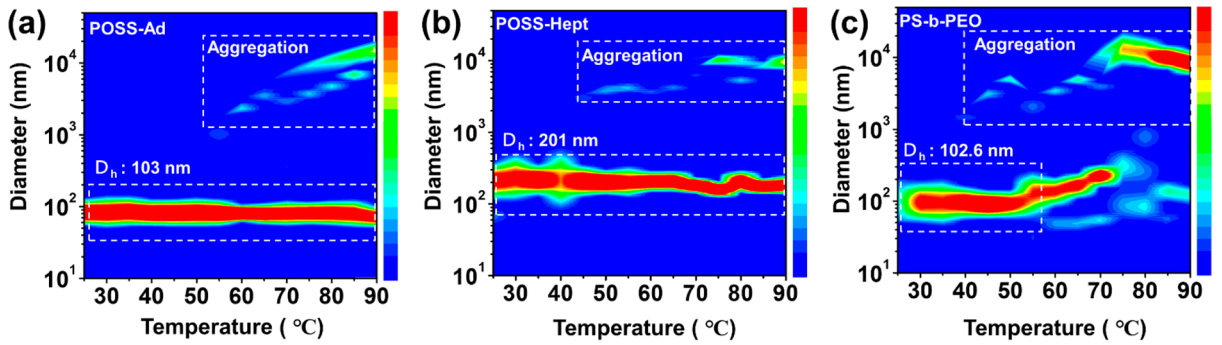

Figure 7. Temperature-dependent size distribution of (a) **POSS-Ad**, (b) **POSS-Hept**, and (c) **PS-*b*-PEO** NPs from the DLS analysis.

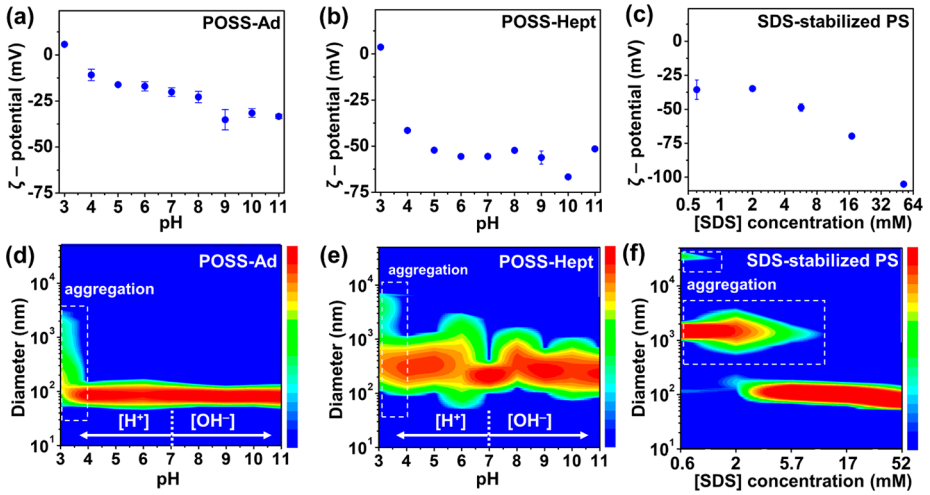

Figure 8. pH-dependent ζ of the (a) **POSS-Ad** and (b) **POSS-Hept** colloidal solutions and ζ of (c) SDS-stabilized PS with different amounts of SDS. pH-dependent size distribution of the (d) **POSS-Ad** and (e) **POSS-Hept** colloidal solutions and the size distribution of (f) SDS-stabilized PS with different amounts of SDS.

Figure 5 show the corresponding ζ changes of the colloidal solutions in the titration experiments. It can be found that added *o*-xylene$_{(l)}$ significantly decreased ζ of the **POSS-Ad** NPs (from −20.1 to −48.9 mV) but slightly increased ζ of the **POSS-Hept** NPs (from −56.9 to −52.9 mV). Because ζ of hydrophobic NPs has a postive correlation to the hydrophobic surface area of the NPs,[17] the distinct changes in the SC Raman spectra and ζ of the two **POSS-(R)$_8$** NPs suggest that added *o*-xylene$_{(l)}$ caused different morphological changes to the **POSS-Ad** and **POSS-Hept** NPs.

To better understand the different morphological influences caused by added *o*-xylene, we summarized the above experimental observations and proposed the two models illustrated in Figure 6. The illustration in panels a and b of Figure 6 shows that added *o*-xylene$_{(l)}$ expelled more SC water from the **POSS-Ad** NPs than the **POSS-Hept** NPs, as indicated by the SC Raman spectra in panels a and b of Figure 5. The results indicate that added *o*-xylene$_{(l)}$ can easily enter the wider hydrophobic pores of the **POSS-Ad** NPs but become clogged at the narrower pores of the **POSS-Hept** NPs, as illustrated in panels c and d of Figure 6. The filled pores of the **POSS-Ad** NPs induce more negative ζ values for the colloidal solution, whereas added *o*-xylene$_{(l)}$ clogged all of the way to the surface of the **POSS-Hept** NPs, resulting in a small local curvature to slightly reduce ζ of the **POSS-Hept** NPs.[29] The distinct morphological modification caused by added *o*-xylene$_{(l)}$ eventually led to the different changes in the morphological stability, where the **POSS-Ad** NPs maintained their morphological stability but the **POSS-Hept** NPs lost their porous morphological feature and behaved similarly to the small molecule oil droplets in the literature[17] that still aggregate even with highly negative ζ, as illustrated in panels e and f of Figure 6. The morphological features of the hydrophobic **POSS-(R)$_8$** NPs also resulted in an unexpected stabilization mechanism that is not included in the classical DLVO theory. Figure 7 shows the temperature-dependent size distribution of the two **POSS-(R)$_8$** and the **PS-*b*-PEO** NPs. The two **POSS-(R)$_8$** NPs show much better thermal stability than the **PS-*b*-PEO** NPs because they maintained their particle sizes up to 90 °C and gave less population of the aggregated particles. In contrast, in Figure 7c, the particle size of the **PS-*b*-PEO** NPs starts to increase at T > 50 °C, and nearly all NPs aggregated into large particles at T > 70 °C. The steric effect in the DLVO theory is generally used to explain the colloidal stability of **PS-*b*-PEO**, in which the steric hindrance provided by the hydrophilic PEO chains prevents the NPs from aggregation. This stabilization mechanism fails at high temperatures because the solubility of PEO in water decreases with the temperature and, above its lower critical solution temperature (LSCT), the PEO phase separates from water; therefore, the **PS-*b*-PEO** NPs lose the steric effect to prevent aggregation.[41] The thermal stability of the two **POSS-(R)$_8$** NPs, on the other hand, is remarkable, because the **POSS-Ad** and **POSS-Hept** NPs rely on their morphological features

https://doi.org/10.1021/acs.langmuir.2c02582
Langmuir 2023, 39, 2922−2931

rather than the hydrophilic protecting shell to prevent aggregation.

Although the hydrophobic **POSS-(R)$_8$** NPs are mainly stabilized by their morphological features, because they still possess negative ζ, electrostatic repulsion might also contribute to the stability. In the literature, the origin of negative ζ of hydrophobic NPs was generally attributed to the surface-absorbed OH^- ion,[17] which can be neutralized by proton ions.[18,21] To examine the contribution of the electrostatic repulsion in the colloidal stability of **POSS-(R)$_8$** NPs, the colloidal solutions of **POSS-Ad** and **POSS-Hept** (pH 7) were titrated by 1 M $HCl_{(aq)}$ and 1 M $NaOH_{(aq)}$, and their ζ and size distribution were measured at different pH values. It can be seen in panels a and b of Figure 8 that added $HCl_{(aq)}$ neutralized ζ of the **POSS-Ad** and **POSS-Hept** colloidal solutions and the isoelectric point was reached at pH ∼ 3.

ζ of the sodium dodecyl sulfate (SDS)-stabilized PS NPs was also measured and shown in Figure 8c. Negative ζ of the SDS-stabilized PS NPs originated from the ionic head groups of the surface-absorbed SDS molecules and is dependent upon the [SDS] concentration in the aqueous solution. In panels d and e of Figure 8, upon reaching the isoelectric point (pH ∼ 3), both the **POSS-Ad** and **POSS-Hept** NPs aggregated, indicating that the electrostatic repulsion does contribute to the colloidal stability of the **POSS-(R)$_8$** NPs. Nevertheless, the morphological factor of the **POSS-Ad** NPs still keeps the colloidal stability quite well before the colloidal solution reaches the isoelectric point, because the **POSS-Ad** colloidal solution maintains the size distribution of NPs in the pH range of 4−11 (see Figure 8d). Nevertheless, in the same pH range, the size distribution of the **POSS-Hept** NPs was broadened by the addition of $HCl_{(aq)}$ or $NaOH_{(aq)}$ (see Figure 8e). Although ζ of the **POSS-(R)$_8$** NPs was not neutralized in this pH range, the addition of $HCl_{(aq)}$ or $NaOH_{(aq)}$ did increase the ionic strength of the colloidal solutions, which weakens the electrostatic repulsion as a result of the high ionic content.[42] In this case, the **POSS-Ad** NPs, which have a less negative ζ and rely more on the morphological stability, demonstrate better colloidal stability to resist the changes in the pH and ionic strength. In contrast, the SDS-stabilized PS NPs follow the classical DLVO theory. As seen in Figure 8f, as a result of the decrease of the [SDS], the SDS-stabilized PS NPs aggregated at $\zeta < |-40|$ mV, indicating that the electrostatic repulsion does dominate the colloidal stability of the SDS-stabilized PS NPs. Assuming that the two **POSS-(R)$_8$** NPs also follow the classical DLVO theory, their stability should be very sensitive to either the ζ or temperature changes. Nevertheless, the **POSS-Ad** NPs retain their colloidal stability at $\zeta \sim 10$ mV or at high temperatures. The extraordinary thermal and pH stability of the **POSS-Ad** NPs thus make **POSS-Ad** a unique colloidal system that requires only a minimal amount of electrostatic repulsion (ζ of −10.9 mV) but no steric effect to be stabilized.

CONCLUSION

Although hydrophobic NPs were normally considered to be unstable in water, our study shows that the hydrophobic NPs of the star-shaped giant molecule, **POSS-(R)$_8$**, utilize their morphological feature to maintain their kinetic stability. Instead of reliance on the electrostatic repulsion and steric effect in the DLVO theory, the hydrophobic NPs of **POSS-(R)$_8$** are stabilized by preventing the entropically driven aggregation caused by the hydrophobic effect. The porous morphology of the **POSS-Ad** NPs allows them to maintain colloidal stability with a minimum ζ and provides the NPs with good encapsulation characteristics and great resistances to the changes in the temperature, pH values, and ionic strength. The study thus shows that the morphological stability of hydrophobic porous NPs is one of the missing pieces in the mechanism of colloidal stability that is a supplement to the classical DLVO theory.

EXPERIMENTAL SECTION

Materials. 4-(Dimethylamino)pyridinium 4-toluenesulfonate (DPTS) was prepared according to a literature procedure. All other reagents and solvents were purchased from commercial sources and were used without purification. If necessary, solvents and reagents were degassed by purging with nitrogen. ^{1}H and ^{13}C nuclear magnetic resonance (NMR) spectra were recorded on an Agilent Unity-400 NMR spectrometer (400 MHz for ^{1}H and 101 MHz for ^{13}C), which used $CDCl_3$ as d solvents to identify the molecular structures at 25 °C. The synthetic details and ^{1}H and ^{13}C NMR and mass spectra can be found in the Supporting Information.

DLS Analysis. DLS was performed using a zeta potential and particle size analyzer ELSZ-2000 series (Otsuka Electronics Co., Ltd.) with a laser wavelength of 633 nm at a fixed angle of 90°.

Confocal Raman Spectroscopy. Raman spectra were recorded on a laboratory-built confocal Raman microspectrometer. The Raman excitation light source was a 632.8 nm He−Ne laser. The laser beam was introduced to an inverted microscope (TE2000, Nikon) and focused onto the sample with a 40× objective lens. A 75 μm pinhole was used in the collection path to obtain a confocal configuration. The collected backscattered light was dispersed using an imaging spectrograph (iHR320, HORIBA Scientific) and recorded using a back-illuminated, liquid N_2-cooled charge-coupled device (CCD) detector (Spec-10:100, Princeton Instruments). The laser power at the sample was around 10 mW. The exposure time for the Raman measurement was 5 min with an acquisition of three spectra per sample. A single quartz cuvette was employed for all of the samples. Sample solutions were prepared and sealed in the cuvette prior to Raman measurements. The optical setup and data analysis procedure details can be found in the Supporting Information.

Zeta Potential (ζ) Measurement. All potential measurements were also performed using zeta potential and particle size analyzer ELSZ-2000 series (Otsuka Electronics Co., Ltd). Henry's equation (shown below) and Smoluchowski approximation were used to calculate ζ from the electrophoretic mobility. The reported ζ values are an average of five measurements, each of which was obtained over 20 electrode cycles

Henry's equation

$$U_E = \frac{2\varepsilon\zeta f(\kappa a)}{3\eta}$$

where U_E is the electrophoretic mobility, ε is the dielectric constant, ζ is the zeta potential, η is the viscosity, and $f(\kappa a)$ is Henry's function.

Preparation of Aqueous Colloids. The aqueous colloids in THF/water with a volume ratio (VR) of 0.10 were prepared following the previous report by Murshid and Wang.[43] Briefly, deionized water (10 mL) was quickly added to the solution of POSS-(R)$_8$ in THF (1 mL, 0.1 mg), resulting in colloidal solutions that have a bluish tint. THF in the as-prepared solution was removed by dialysis against water. The Raman spectra of the solutions were measured to probe whether THF was completely removed.

Preparation of POSS-(R)$_8$ NPs with Different pH. The pH of the aqueous solution of the **POSS-(R)$_8$** NPs was adjusted by adding 100 μL of hydrogen chloride (HCl) or sodium hydroxide (NaOH) aqueous solutions into 900 μL of the aqueous solution of **POSS-(R)$_8$** NPs. The pH values of $HCl_{(aq)}$ were adjusted from pH 2 to 5, and the pH values of $NaOH_{(aq)}$ were adjusted from pH 8 to 10 before being added to the aqueous solution of the **POSS-(R)$_8$** NPs.

https://doi.org/10.1021/acs.langmuir.2c02582
Langmuir 2023, 39, 2922−2931

Preparation of the SDS-Stabilized Polystyrene. SDS (150 mg) was dissolved in water (10 mL). The initiator azobisisobutyronitrile (AIBN, 12.5 mg) and styrene monomer (1.25 mL) were then added. The mixture was chilled under an ice bath and further emulsified by a VibraCell ultrasonic processor (Sonics and Materials, Inc.) with a standard probe at 40% amplitude for 2 min. The emulsion polymerization was carried out in a glass vessel under N_2 at 70 °C for 12 h. The size distribution of the SDS-stabilized polystyrene NPs was determined by the DLS measurement. To control the concentration of SDS, the colloidal solution (45 mL) was centrifuged at 12000 rpm for 10 min. After centrifugation, a certain amount of supernatant was taken away and replaced by an equal amount of deionized water to reduce the concentration of SDS. The colloidal solutions that have lower concentrations of SDS were then sonicated by an ultrasonic cleaner (Delta Ultrasonic Co., Ltd.) for 1 min and left to stand for 1 day before the following DLS measurement.

■ ASSOCIATED CONTENT

Supporting Information

The Supporting Information is available free of charge at https://pubs.acs.org/doi/10.1021/acs.langmuir.2c02582.

Detailed synthesis, structural characterization methods, analyses, and instrumentation (PDF)

■ AUTHOR INFORMATION

Corresponding Authors

Xiaosong Wang − *Department of Chemistry, Waterloo University, Waterloo, Ontario N2L 3G1, Canada;* orcid.org/0000-0002-6415-4768; Email: xiaosong.wang@uwaterloo.ca

Chien-Lung Wang − *Department of Applied Chemistry, National Yang Ming Chiao Tung University, Hsinchu 30010, Taiwan;* orcid.org/0000-0002-4799-4730; Email: kclwang@nycu.edu.tw

Authors

Chin-Yi Chen − *Department of Applied Chemistry, National Yang Ming Chiao Tung University, Hsinchu 30010, Taiwan*

Meng-Ju Hsieh − *Department of Applied Chemistry, National Yang Ming Chiao Tung University, Hsinchu 30010, Taiwan*

Ankit Raj − *Department of Applied Chemistry, National Yang Ming Chiao Tung University, Hsinchu 30010, Taiwan;* orcid.org/0000-0002-2495-3354

Wei-Cheng Peng − *Department of Applied Chemistry, National Yang Ming Chiao Tung University, Hsinchu 30010, Taiwan*

Hiro-o Hamaguchi − *Department of Applied Chemistry, National Yang Ming Chiao Tung University, Hsinchu 30010, Taiwan*

Wei-Tsung Chuang − *National Synchrotron Radiation Research Center, Hsinchu 30076, Taiwan;* orcid.org/0000-0002-9000-2194

Complete contact information is available at: https://pubs.acs.org/10.1021/acs.langmuir.2c02582

Funding

This work was supported in part by the Ministry of Science and Technology, Taiwan (MOST 109-2223-E-009-001-MY3).

Notes

The authors declare no competing financial interest.

■ ACKNOWLEDGMENTS

WAXS experiments were performed at the beamline BL23A1, National Synchrotron Radiation Research Center, Taiwan.

■ REFERENCES

(1) Lewis, J. A. Colloidal processing of ceramics. *J. Am. Ceram. Soc.* **2000**, *83*, 2341−2359.

(2) Agarwal, N.; Farris, R. Mechanical properties of acrylic based latex blend coatings. *Polym. Eng. Sci.* **2000**, *40*, 376−390.

(3) Braun, P. V.; Wiltzius, P. Electrochemically grown photonic crystals. *Nature* **1999**, *402*, 603−604.

(4) Johnson, S. A.; Ollivier, P. J.; Mallouk, T. E. Ordered mesoporous polymers of tunable pore size from colloidal silica templates. *Science* **1999**, *283*, 963−965.

(5) Yablonovitch, E. Inhibited spontaneous emission in solid-state physics and electronics. *Phys. Rev. Lett.* **1987**, *58*, 2059.

(6) Müller, R. H. *Colloidal Carriers for Controlled Drug Delivery and Targeting: Modification, Characterization and In Vivo Distribution*; Routledge (Taylor & Francis Group): Abingdon-on-Thames, U.K., 1991.

(7) De Jong, W. H.; Borm, P. J. Drug delivery and nanoparticles: Applications and hazards. *Int. J. Nanomed.* **2008**, *3*, 133.

(8) Derjaguin, B.; Landau, L. Theory of stability of highly charged lyophobic sols and coalescence of highly charged particles in electrolyte solutions. *Acta Physicochim. URSS* **1941**, *14*, 633−662.

(9) Verwey, E. J. W. Theory of the stability of lyophobic colloids. *J. Phys. Chem.* **1947**, *51*, 631−636.

(10) Napper, D. H. *Polymeric Stabilization of Colloidal Dispersions*; Academic Press: New York, 1983; Vol. 3.

(11) Witten, T.; Pincus, P. Colloid stabilization by long grafted polymers. *Macromolecules* **1986**, *19*, 2509−2513.

(12) *Solid−Liquid Dispersions*; Tadros, T. F., Ed.; Academic Press: London, U.K., 1987.

(13) Kuchibhatla, S. V.; Karakoti, A.; Seal, S. Colloidal stability by surface modification. *Jom* **2005**, *57*, 52−56.

(14) Wijenayaka, L. A.; Ivanov, M. R.; Cheatum, C. M.; Haes, A. J. Improved parametrization for extended Derjaguin, Landau, Verwey, and Overbeek predictions of functionalized gold nanosphere stability. *J. Phys. Chem. C* **2015**, *119*, 10064−10075.

(15) Xi, W.; Phan, H. T.; Haes, A. J. How to accurately predict solution-phase gold nanostar stability. *Anal. Bioanal. Chem.* **2018**, *410*, 6113−6123.

(16) Kumar, A.; Dixit, C. K. Methods for characterization of nanoparticles. In *Advances in Nanomedicine for the Delivery of Therapeutic Nucleic Acids*; Nimesh, Chandra, R., Gupta, N., Eds.; Woodhead Publishing: Sawston, U.K., 2017; Chapter 3, pp 43−58, DOI: 10.1016/B978-0-08-100557-6.00003-1.

(17) Marinova, K.; Alargova, R.; Denkov, N.; Velev, O.; Petsev, D.; Ivanov, I.; Borwankar, R. Charging of oil− water interfaces due to spontaneous adsorption of hydroxyl ions. *Langmuir* **1996**, *12*, 2045−2051.

(18) Beattie, J. K.; Djerdjev, A. M. The pristine oil/water interface: Surfactant-free hydroxide-charged emulsions. *Angew. Chem., Int. Ed. Engl.* **2004**, *43*, 3568−71.

(19) Poli, E.; Jong, K. H.; Hassanali, A. Charge transfer as a ubiquitous mechanism in determining the negative charge at hydrophobic interfaces. *Nat. Commun.* **2020**, *11*, 901.

(20) Scheu, R.; Rankin, B. M.; Chen, Y.; Jena, K. C.; Ben-Amotz, D.; Roke, S. Charge asymmetry at aqueous hydrophobic interfaces and hydration shells. *Angew. Chem., Int. Ed. Engl.* **2014**, *53*, 9560−3.

(21) Pullanchery, S.; Kulik, S.; Okur, H. I.; De Aguiar, H.; Roke, S. On the stability and necessary electrophoretic mobility of bare oil nanodroplets in water. *J. Chem. Phys.* **2020**, *152*, 241104.

(22) Pullanchery, S.; Kulik, S.; Rehl, B.; Hassanali, A.; Roke, S. Charge transfer across C−H··· O hydrogen bonds stabilizes oil droplets in water. *Science* **2021**, *374*, 1366−1370.

(23) Kronberg, B. The hydrophobic effect. *Curr. Opin. Colloid Interface Sci.* **2016**, *22*, 14−22.

(24) Biedermann, F.; Nau, W. M.; Schneider, H. J. The hydrophobic effect revisited–studies with supramolecular complexes imply high-energy water as a noncovalent driving force. *Angew. Chem., Int. Ed. Engl.* **2014**, *53*, 11158−71.
(25) Chandler, D. Interfaces and the driving force of hydrophobic assembly. *Nature* **2005**, *437*, 640−647.
(26) Lan, Y.; Caciagli, A.; Guidetti, G.; Yu, Z.; Liu, J.; Johansen, V. E.; Kamp, M.; Abell, C.; Vignolini, S.; Scherman, O. A.; Eiser, E. Unexpected stability of aqueous dispersions of raspberry-like colloids. *Nat. Commun.* **2018**, *9*, 3614.
(27) Pashley, R. Effect of degassing on the formation and stability of surfactant-free emulsions and fine Teflon dispersions. *J. Phys. Chem. B* **2003**, *107*, 1714−1720.
(28) Alargova, R. G.; Deguchi, S.; Tsujii, K. Stable colloidal dispersions of fullerenes in polar organic solvents. *J. Am. Chem. Soc.* **2001**, *123*, 10460−10467.
(29) Alan, B. O.; Barisik, M.; Ozcelik, H. G. Roughness effects on the surface charge properties of silica nanoparticles. *J. Phys. Chem. C* **2020**, *124*, 7274−7286.
(30) Yakin, F. E.; Barisik, M.; Sen, T. Pore size and porosity dependent zeta potentials of mesoporous silica nanoparticles. *J. Phys. Chem. C* **2020**, *124*, 19579−19587.
(31) Ando, M.; Hamaguchi, H. Quantitative spectrometry of complex systems by hypothetical addition multivariate analysis. *J. Spectrosc. Soc. Jpn.* **2015**, *64*, 280−284.
(32) Ando, M.; Lednev, I. K.; Hamaguchi, H. Quantitative Spectrometry of Complex Molecular Systems by Hypothetical Addition Multivariate Analysis With Numerical Differentiation (HAMAND). *Front. Mol. Biosci.* **2018**, 369−378.
(33) Okajima, H.; Ando, M.; Hamaguchi, H.-o. Formation of "nano-ice" and density maximum anomaly of water. *Bull. Chem. Soc. Jpn.* **2018**, *91*, 991−997.
(34) Davis, J. G.; Rankin, B. M.; Gierszal, K. P.; Ben-Amotz, D. On the cooperative formation of non-hydrogen-bonded water at molecular hydrophobic interfaces. *Nat. Chem.* **2013**, *5*, 796−802.
(35) Hamaguchi, H. Ordered structures in liquid water: Is cold water a genuine liquid? *J. Raman Spectrosc.* **2022**, *53*, 1656−1665.
(36) Davis, J. G.; Gierszal, K. P.; Wang, P.; Ben-Amotz, D. Water structural transformation at molecular hydrophobic interfaces. *Nature* **2012**, *491*, 582−5.
(37) Perera, P.; Fega, K.; Lawrence, C.; Sundstrom, E.; Tomlinson-Phillips, J.; Ben-Amotz, D. Observation of water dangling OH bonds around dissolved nonpolar groups. *Proc. Natl. Acad. Sci. U. S. A.* **2009**, *106*, 12230−12234.
(38) Chaplin, M. A proposal for the structuring of water. *Biophys. Chem.* **2000**, *83*, 211−221.
(39) Samuel, A. Z.; Lai, B.-H.; Lan, S.-T.; Ando, M.; Wang, C.-L.; Hamaguchi, H.-o. Estimating percent crystallinity of polyethylene as a function of temperature by Raman spectroscopy multivariate curve resolution by alternating least squares. *Anal. Chem.* **2017**, *89*, 3043−3050.
(40) Okubo, M.; Shiozaki, M.; Tsujihiro, M.; Tsukuda, Y. Preparation of micron-size monodisperse polymer particles by seeded polymerization utilizing the dynamic monomer swelling method. *Colloid Polym. Sci.* **1991**, *269*, 222−226.
(41) Grinberg, V. Y.; Burova, T. V.; Grinberg, N. V.; Dubovik, A. S.; Papkov, V. S.; Khokhlov, A. R. Energetics of LCST transition of poly(ethylene oxide) in aqueous solutions. *Polymer* **2015**, *73*, 86−90.
(42) Evans, D. F.; Wennerström, H. *The Colloidal Domain: Where Physics, Chemistry, Biology, and Technology Meet*, 2nd ed.; Wiley-VCH: Weinheim, Germany, 1999.
(43) Murshid, N.; Wang, X. Iron−Carbonyl Aqueous Vesicles (MCsomes) by Hydration of $[Fe(CO)\{CO(CH_2)_5CH_3\}(Cp)(PPh_3)]$ (FpC_6): Highly Integrated Colloids with Aggregation-Induced Self-Enhanced IR Absorption (AI-SEIRA). *Chemistry* **2015**, *21*, 19223−30.

https://doi.org/10.1021/acs.langmuir.2c02582
Langmuir 2023, 39, 2922−2931